



# Synthesis of Tb<sup>3+</sup> ion doped ZnWO<sub>4</sub> phosphors and investigation of their photoluminescence properties: concentration effect

N PREMJJIT SINGH<sup>1,2,\*</sup>, Y RANGEELA DEVI<sup>3</sup>, N RAJMUHON SINGH<sup>4</sup>  
and N MOHONDAS SINGH<sup>1</sup>

<sup>1</sup>Department of Chemistry, Mizoram University, Aizawl 796004, India

<sup>2</sup>Department of Chemistry, A. R. S. D. College, University of Delhi, New Delhi 110021, India

<sup>3</sup>Department of Physics, Pachhunga University College, Aizawl 796001, India

<sup>4</sup>Department of Chemistry, Manipur University, Imphal 795003, India

\*Author for correspondence (premjit.naorem@yahoo.in)

MS received 20 May 2018; accepted 9 October 2018; published online 27 March 2019

**Abstract.** In this paper, the effects of Tb<sup>3+</sup> ion concentration on the structural and photoluminescence properties of ZnWO<sub>4</sub>:Tb<sup>3+</sup> have been reported. X-ray diffraction studies indicated that the monoclinic structure of the samples and the crystallinity were found to decrease with the increase of Tb<sup>3+</sup> ion concentration due to the distortion in the crystal lattice. The formation of the monoclinic structure was further supported by high resolution transmission electron microscopy and Fourier transform infrared analyses. The transmission electron microscopy image of ZnWO<sub>4</sub>:Tb<sup>3+</sup> (7%) showed a spherical morphology with crystallite sizes in the range of ~8–12 nm. The excitation spectrum showed a strong broad band originated from the electronic transition within the WO<sub>6</sub><sup>6-</sup> group. Upon excitation at 270 nm, the prepared ZnWO<sub>4</sub>:Tb<sup>3+</sup> phosphors exhibited sharp and narrow emission peaks, characteristic of the f–f transitions of Tb<sup>3+</sup> ions besides a broad band with the maximum at around 460 nm due to the host lattice. The intensity of the broad emission band was found to decrease gradually with the increase of Tb<sup>3+</sup> ion concentration and reached minimum at 7 at%. The decay time of the prepared phosphors was investigated in detail and the maximum average lifetime value is found to be 1.187 ms.

**Keywords.** ZnWO<sub>4</sub>:Tb<sup>3+</sup>; photoluminescence; concentration effect.

## 1. Introduction

Research on the luminescence properties of rare earth ion activated inorganic nanomaterials has increased in the last few years due to their potential applications in lighting and display devices, including plasma display panels, white light emitting diodes (WLEDs), fluorescence lamps, cathode ray tubes, and so on [1,2]. For the host material, tungstate compounds are considered as good candidates due to their many precious properties like high thermal and chemical stabilities, long afterglow to luminescence, high average refractive index, non-toxicity, non-hygroscopicity and high light yield [3–5]. Besides, the excited tungstate group can transfer the energy effectively to the rare earth ions [6,7]. ZnWO<sub>4</sub> (Sanmarite) is one of the members of the tungstate family which is a very attractive material due to its exciting luminescence, physical, chemical and structural properties as well as its potential applications in a variety of fields such as in photoluminescence, photo-catalysis, sensing, microwave, X-ray and  $\gamma$ -scintillation, phase change optical recording media and acoustic and optical fibres [8–12]. It crystallizes in the monoclinic wolframite structure with a  $C_{2h}$  point group symmetry and space group of  $P2_1/C$  [13]. In this structure, both the cations Zn<sup>2+</sup> and W<sup>6+</sup> are coordinated by six surrounding

oxygen atoms and a distorted octahedral geometry of ZnO<sub>6</sub> and WO<sub>6</sub> is formed [13]. Several methods are applied for the synthesis of rare earth ion activated inorganic phosphors such as solid state reactions, Czochralski process, co-precipitation, sol–gel and hydrothermal methods and so on. Among them, the co-precipitation method is very attractive due to its simplicity, low cost and low time consumption [14]. It is also well known that the size and morphology of a phosphor are important parameters since the luminescence dynamics are tuned by these parameters [1,15]. An organic ligand can be used as a solvent in the synthesis to tune the particle size and morphology as well as to prevent the agglomeration [14]. It is also reported in the literature that the use of a long chain ligand may cause quenching of luminescence due to the high vibrational energy of the ligand [16]. Therefore, in this present investigation, the nanocrystals of ZnWO<sub>4</sub>:Tb<sup>3+</sup> phosphors have been prepared by the co-precipitation method using a short chain ligand ethylene glycol as the capping agent and the reaction medium.

Upto now, many studies on the luminescence properties of lanthanide ion doped ZnWO<sub>4</sub> have been reported. But most of the studies were mainly focused on the doping of rare earth ions such as Eu<sup>3+</sup> [3,17–20] and Sm<sup>3+</sup> [6,21,22] ions and doping with other rare earth ions such as

Tb<sup>3+</sup> ions is rarely investigated. On the other hand, trivalent terbium is a green colour producing rare earth ion due to its <sup>5</sup>D<sub>4</sub>–<sup>7</sup>F<sub>J=3,4,5,6</sub> transitions and it has been widely used in green phosphor. Moreover, this ion shows high quantum efficiency and high stability and is suitable for application in light emitting diodes [1]. Green colour is also one of the key components of tri-colour luminescence and therefore can be applied in the development of WLEDs. Liao *et al* [23] already reported the effect of charge compensators such as Li<sup>+</sup>, K<sup>+</sup> and Na<sup>+</sup> on the luminescence properties of ZnWO<sub>4</sub> doped with Tb<sup>3+</sup> ions synthesized by the hydrothermal method. However, the concentration of dopant ions is also one of the parameters which can induce a strong influence on the luminescence properties. Therefore, the present paper is mainly focused on the concentration dependent luminescence behaviour of ZnWO<sub>4</sub>:Tb<sup>3+</sup> phosphors synthesized by the co-precipitation method. To the best of author's knowledge there has not yet been any report similar to our work.

## 2. Experimental

### 2.1 Sample preparation

In this investigation, the synthesis of Tb<sup>3+</sup> ion doped ZnWO<sub>4</sub> nanocrystals was carried out by the co-precipitation method using ethylene glycol as the capping agent and the reaction medium followed by annealing of the precipitates formed at 500°C for 2 h. In the synthesis of ZnWO<sub>4</sub>:xTb<sup>3+</sup> (x = 1, 3, 5, 7, 10 and 12 at%) phosphors, the stoichiometric amounts of ZnCl<sub>2</sub> · xH<sub>2</sub>O (Thomas Baker, 98%) and TbCl<sub>3</sub> · xH<sub>2</sub>O (Alpha Aesar, 99.99%) were dissolved together in 25 ml ethylene glycol solvent in a round bottom flask. The Na<sub>2</sub>WO<sub>4</sub> (Himedia, 99%) solution prepared in 25 ml ethylene glycol was added into the above solution, and then the mixed solution was refluxed at a temperature of 180°C for 3 h. The obtained white colour precipitate was then centrifuged and washed with double distilled water for about five times and finally with acetone. After this, the precipitate was dried in an oven at a temperature of 60–70°C for about 24 h, and then annealed in a muffle furnace.

### 2.2 Characterization of the samples

The prepared samples were characterized using different characterization techniques. For the characterization of phase composition and the crystal structure of the prepared samples, PANalytical powder X-ray diffraction (XRD) with Cu Kα (1.5405 Å) radiation and a Ni filter was used. Vibrational spectra were recorded by using a Perkin Elmer FT-IR RXI spectrometer in the range of 400–4000 cm<sup>-1</sup> with KBr as a beam splitter. The elemental analysis of the sample was performed by using an energy dispersive analysis of X-ray (EDAX) spectrometer embedded in a FEI Quanta 250 scanning electron microscope (SEM). The transmission electron microscopy (TEM) image, high resolution transmission

electron microscopy image (HRTEM) and selected area electron diffraction (SAED) image of ZnWO<sub>4</sub>:Tb<sup>3+</sup> (7 at%) were recorded using a JEOL (TEM) JEM-2100. For recording the excitation and emission spectra and the decay time of Tb<sup>3+</sup> ion doped ZnWO<sub>4</sub> phosphors, a Hitachi (F-7000) fluorescence spectrophotometer with a xenon discharge lamp was used. All the above measurements were taken at room temperature.

## 3. Result and discussion

### 3.1 XRD studies

Figure 1a shows the XRD patterns of ZnWO<sub>4</sub>:Tb<sup>3+</sup> phosphors with Tb<sup>3+</sup> ion concentrations of 1, 5, 7, 10 and 12 at%. The diffraction peaks of the samples can be indexed to the monoclinic structure of ZnWO<sub>4</sub> (JCPDS card number 15-0774) having cell constants  $a = 4.691$  Å,  $b = 5.720$  Å,  $c = 4.925$  Å and volume (V) = 132.14 Å<sup>3</sup>. The larger diffraction peak width of the samples seen in the figure as compared to the diffraction peak width of standard ZnWO<sub>4</sub> for the bulk material indicates that the prepared samples have a fine crystallite size. In order to evaluate the effect of the Tb<sup>3+</sup> ion concentration on crystallization, the most intense (111) peak is zoomed out in the 2θ range from 25 to 35° and is shown in figure 1b. A gradual decrease of peak intensity could be clearly seen with the increase of the Tb<sup>3+</sup> ion concentration up to 7%, which implies that the crystal quality is deteriorating. This continuous deterioration of the crystal quality with the increase of the Tb<sup>3+</sup> ion concentration might be due to the substitution of Zn<sup>2+</sup> ions by larger sized Tb<sup>3+</sup> ions. The radii of the cations at co-ordination number six are  $r_{Zn^{2+}} = 0.74$  Å and  $r_{Tb^{3+}} = 0.923$  Å, respectively [24]. Similar crystalline growth inhibition was also reported by Nguyen *et al* [6] in the ZnWO<sub>4</sub>:Sm<sup>3+</sup> phosphor synthesized by the hydrothermal method. However, when the concentration of Tb<sup>3+</sup> ions is increased to 10 and 12%, the peak intensity is further increased slightly, which means that the crystal quality is increasing. Shifting of the peak slightly towards the lower 2θ angle (figure 1b) and a gradual increase in the cell volume (table 1) with the increase of Tb<sup>3+</sup> ion concentration are also observed. All these results have supported the substitution of Zn<sup>2+</sup> by larger sized Tb<sup>3+</sup> ions. Table 1 shows the calculated lattice constants and cell volumes along with crystallite sizes of the samples. The cell volume and lattice constants were calculated using a program UnitCellWin and the crystallite sizes were evaluated using the Scherrer equation:  $D = 0.9\lambda/\beta\cos\theta$ , where  $D$  is the crystallite diameter,  $\beta$  is the full width at half maximum in radians,  $\lambda$  is the wavelength of X-ray used (1.054 Å) and  $\theta$  is the angle of diffraction.

### 3.2 FT-IR study

Figure 2 shows the FT-IR spectra of ZnWO<sub>4</sub>:Tb<sup>3+</sup> for the Tb<sup>3+</sup> ion concentrations of 3 and 10 at%. It is clearly

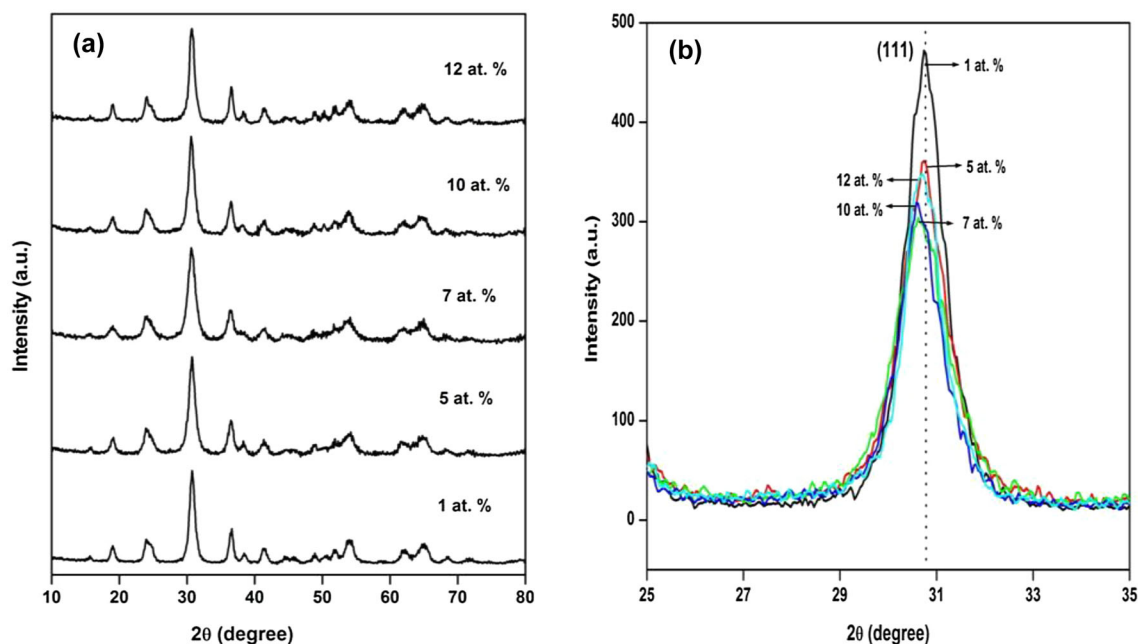


**Figure 1.** (a) XRD patterns of  $\text{ZnWO}_4$  doped with  $x$  at% of  $\text{Tb}^{3+}$  ions ( $x = 1, 5, 7, 10$  and  $12$ ). (b) Expanded view of the (111) peak showing the variation of intensity and deflection of the peak with concentration.

**Table 1.** Lattice parameters, unit cell volumes and crystallite sizes of  $\text{ZnWO}_4:\text{Tb}^{3+}$  phosphors.

Dopant ions (at%)	Lattice parameters			Cell volume (V) $\text{\AA}^3$	Crystallite size (nm)
	$a$ ( $\text{\AA}$ )	$b$ ( $\text{\AA}$ )	$c$ ( $\text{\AA}$ )		
1 ( $\text{Tb}^{3+}$ )	4.681	5.694	4.924	131.23	11.3
5 ( $\text{Tb}^{3+}$ )	4.696	5.704	4.904	131.35	8.4
7 ( $\text{Tb}^{3+}$ )	4.688	5.695	4.926	131.51	8.4
10 ( $\text{Tb}^{3+}$ )	4.706	5.705	4.899	131.53	9.7
12 ( $\text{Tb}^{3+}$ )	4.689	5.705	4.903	131.18	11.0

seen from this figure that the spectra exhibited bands at around  $3440$  and  $1640\text{ cm}^{-1}$  and that can be ascribed to the stretching and bending vibrational modes of the adsorbed  $\text{H}_2\text{O}$  molecules, respectively, which means that the samples are hydroxylated. Further, there exist bands at  $2965$  and  $1395\text{ cm}^{-1}$  which can be assigned to the stretching and bending vibrational modes of the  $-\text{CH}_2$  group that originated from the solvent ethylene glycol, respectively [25,26]; this result indicates that ethylene glycol has not been removed completely from the samples. Many peaks are also observed in between  $500$  and  $900\text{ cm}^{-1}$  and that are the characteristic peaks of the tungstate group. The strong bands found at  $880$  and  $833\text{ cm}^{-1}$  correspond to the stretching and bending vibrational modes of  $\text{Zn}-\text{O}-\text{W}$  bonds whereas the bands found at  $692$  and  $623\text{ cm}^{-1}$  are due to the stretching and bending vibrational modes of the  $\text{W}-\text{O}$  bond. Bands observed at  $521$  and  $458\text{ cm}^{-1}$  correspond to the stretching and bending vibrational modes of  $\text{Zn}-\text{O}$  bonds. These vibrational modes agreed well with those reported in the literature [8,27]. From this study, it is revealed that the prepared sample is the desired compound.

### 3.3 TEM studies

The TEM image of  $\text{ZnWO}_4:\text{Tb}^{3+}$  (7 at%) is shown in figure 3a. The image shows a spherical morphology without agglomeration and the crystallite diameter was varied in the range of  $8\text{--}12\text{ nm}$ , which agrees well with the value calculated from XRD. A phosphor having a spherical morphology leads to high brightness due to its high packing density and low scattering of light [28,29]. Furthermore, the sample was subjected to HRTEM in order to see the crystallinity and purity. Figure 3b and c show the HRTEM image and SAED pattern of  $\text{ZnWO}_4:\text{Tb}^{3+}$  (7 at%), respectively. The HRTEM image shows a clear picture of the interplanar lattice fringes and the distances  $3.03$  and  $2.38\text{ \AA}$  shown in the figure correspond to the (111) and (021) planes, respectively, which further indicates the formation of the monoclinic structure of the sample. The SAED pattern shown in figure 3c is composed of dotted rings, indicating the formation of polycrystallinity of the sample. The EDAX spectrum of  $\text{ZnWO}_4:\text{Tb}^{3+}$  (7 at%) is shown in figure 3d, which consists of peaks corresponding

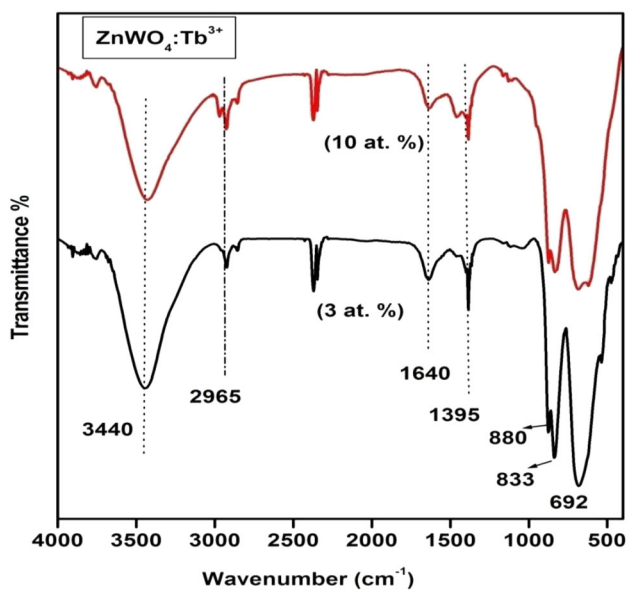


**Figure 2.** FT-IR spectra of  $\text{ZnWO}_4:\text{Tb}^{3+}$  with the concentrations of 3 and 10 at%.

to Zn, W, O and Tb, indicating that the prepared sample contains the required elements.

### 3.4 Photoluminescence studies

The excitation spectrum of  $\text{ZnWO}_4:\text{Tb}^{3+}$  (7 at%) obtained by monitoring the emission wavelength at 545 nm is shown in figure 4a. The spectrum consists of a strong and broad band in the wavelength range between 230 and 320 nm with a maximum at around 270 nm. This broad band can be ascribed to the charge transfer transitions due to the electronic excitation from the filled 2p orbital of the oxygen ligand to the empty 5d orbital of tungsten ions inside the  $\text{WO}_6^{6-}$  group [4,23]. In addition, the spectrum also exhibited sharp and narrow peaks of weak intensity towards the longer wavelength regions i.e., beyond 320 nm. These narrow peaks are scarcely seen because of low intensity; therefore, in order to see clearly, the spectrum is expanded in the wavelength ranging from 325 to 400 nm and is shown in figure 4b. These narrow peaks are induced by the excitation of electrons from the ground state energy level ( $^7F_6$ ) to various excited states of  $\text{Tb}^{3+}$  ions within the

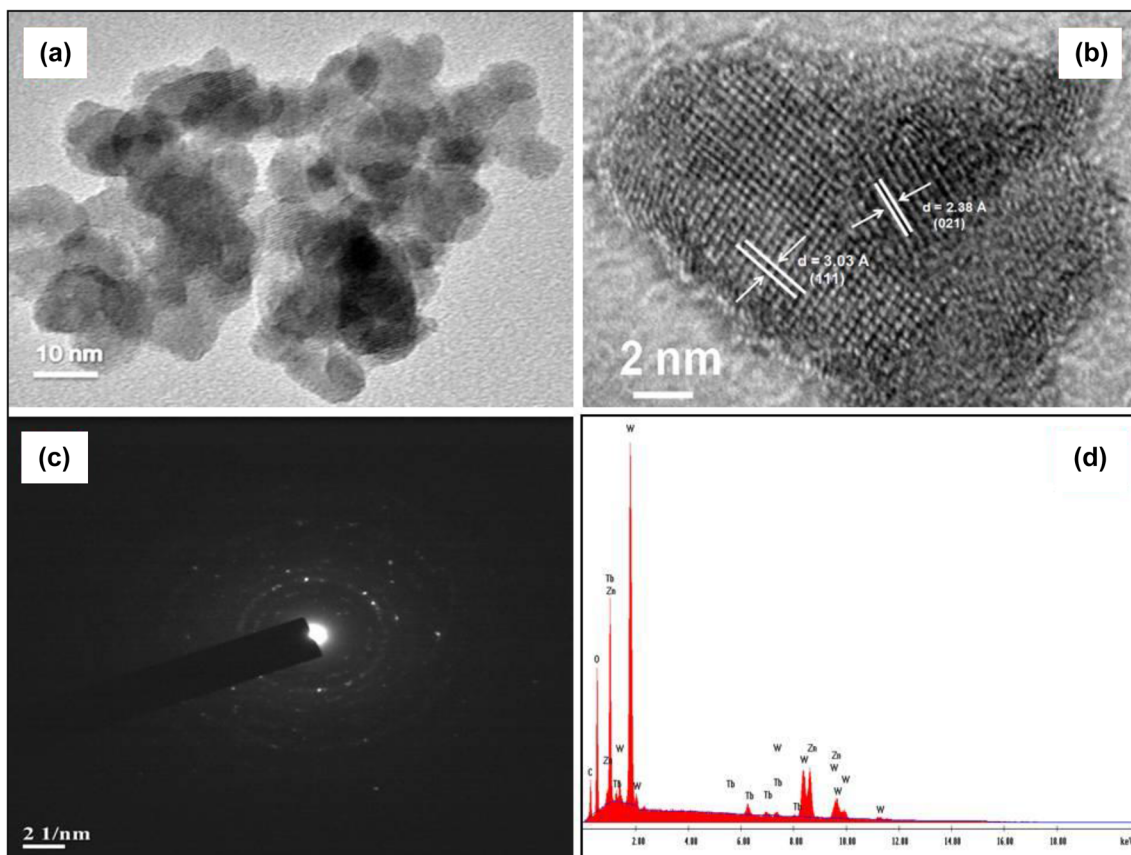


**Figure 3.** (a) TEM image, (b) HRTEM image, (c) SAED pattern and (d) EDAX spectra of  $\text{ZnWO}_4:\text{Tb}^{3+}$  (7 at%) phosphor.

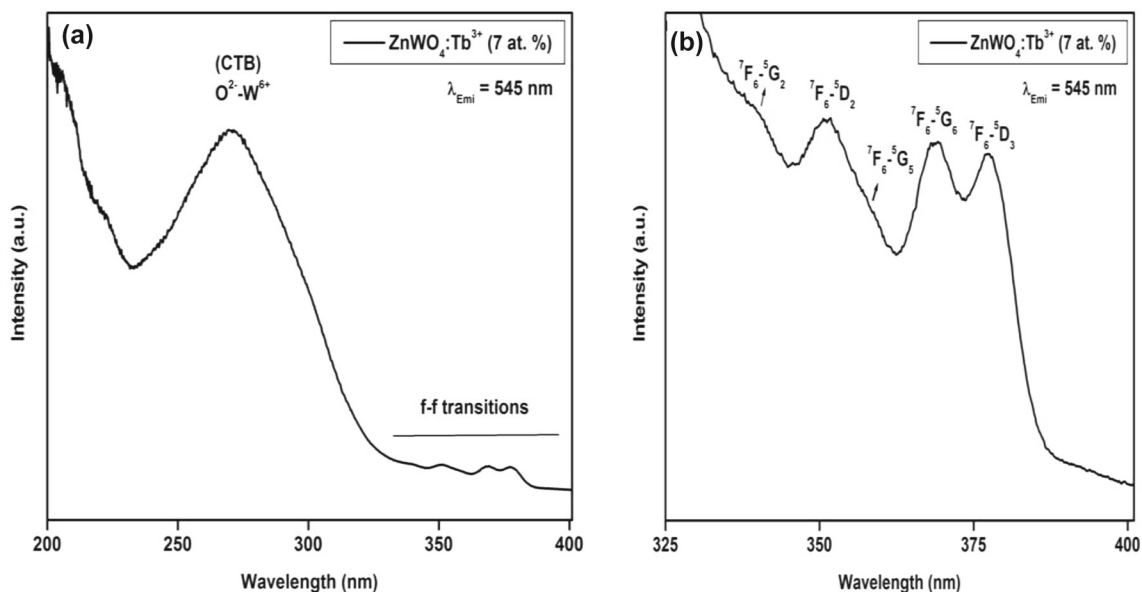


**Figure 4.** (a) Excitation spectrum of  $\text{ZnWO}_4:\text{Tb}^{3+}$  (7 at.%) phosphor. (b) Expansion of the spectrum in the wavelength ranges from 325 to 400 nm.

4f energy levels. These narrow peaks centre at 340, 351, 359, 369 and 377 nm and can be ascribed to the  ${}^7\text{F}_6-{}^5\text{G}_2$ ,  ${}^7\text{F}_6-{}^5\text{D}_2$ ,  ${}^7\text{F}_6-{}^5\text{G}_5$ ,  ${}^7\text{F}_6-{}^5\text{G}_6$  and  ${}^7\text{F}_6-{}^5\text{D}_3$  transitions, respectively [23, 30]. The presence of the strong broad absorption band due to the host lattice in the excitation spectrum indicates the existence of efficient energy transfer from the host lattice to the  $\text{Tb}^{3+}$  ions. In order to further see the energy transfer from the host lattice, the emission spectra of  $\text{ZnWO}_4:\text{Tb}^{3+}$  (7 at.%) have been recorded under various excitation wavelengths such as 270, 340, 351, 369 and 377 nm and are shown in figure 5a. The excitation wavelength 270 nm is called indirect excitation (host lattice) because the electronic transition involved here is within the  $\text{WO}_6^{6-}$  group of the host lattice whereas 340, 351, 369 and 377 nm are called direct excitation since the transitions involved is within the 4f electrons of  $\text{Tb}^{3+}$  ions. It is revealed from figure 5a that the strongest intensity is observed upon excitation at 270 nm; this result further supported the effective energy transfer from the host lattice to the  $\text{Tb}^{3+}$  ions. The spectra consist of emission peaks originating from the  ${}^5\text{D}_3$  and  ${}^5\text{D}_4$  energy states with little background emission from the host lattice; the peaks observed in the range between 400 and 467 nm originate from the  ${}^5\text{D}_3$  state and can be ascribed to the  ${}^5\text{D}_3-{}^7\text{F}_5$  (423 nm),  ${}^5\text{D}_3-{}^7\text{F}_4$  (437 nm),  ${}^5\text{D}_3-{}^7\text{F}_3$  (45 nm) and  ${}^5\text{D}_3-{}^7\text{F}_2$  (467 nm) transitions whereas the peaks centred at 489, 544, 585 and 621 nm originate from the  ${}^5\text{D}_4$  state and they can be attributed to the  ${}^5\text{D}_4-{}^7\text{F}_6$ ,  ${}^5\text{D}_4-{}^7\text{F}_5$ ,  ${}^5\text{D}_4-{}^7\text{F}_4$  and  ${}^5\text{D}_4-{}^7\text{F}_3$  transitions, respectively [16,31,32].

Figure 5b shows the emission spectra of  $\text{ZnWO}_4:x\text{Tb}^{3+}$  ( $x = 1, 3, 5, 7, 10$  and 12 at.%) obtained by monitoring the excitation wavelength at 270 nm, this wavelength was chosen because the strongest emission was observed upon excitation at this wavelength. In addition to sharp and narrow peaks of

dopant  $\text{Tb}^{3+}$  ions, the spectra also consist of a broad band with a maximum at around 460 nm in the blue region. This broad band is due to the overlapping of intrinsic luminescence of the host lattice and the emissions originating from the  ${}^5\text{D}_3$  state of  $\text{Tb}^{3+}$  ions as the two transitions fall in the same region. The intrinsic luminescence of the host lattice is induced by the electronic transition  ${}^3\text{T}_{1u} \rightarrow {}^1\text{A}_{1g}$  within the  $\text{WO}_6^{6-}$  complex plus the recombination of e-h pairs located at the tungsten ions that have deficient oxygen atoms [8,33]. It is seen from figure 5b that the intensity of the broad band decreases gradually with the increase of  $\text{Tb}^{3+}$  ion concentration and becomes the weakest at 7%. Due to this progressive quenching of the broad emission band originating from the host lattice, the emission intensity of the peak centred at 544 nm due to the  ${}^5\text{D}_4-{}^7\text{F}_5$  transition of  $\text{Tb}^{3+}$  ions becomes stronger than the broad band of the host lattice at the  $\text{Tb}^{3+}$  concentrations of 5 and 7%. These results imply that the efficiency of energy transfer from the host lattice to the  $\text{Tb}^{3+}$  ions increases with the increase of the  $\text{Tb}^{3+}$  ion concentration and a high efficient energy transfer is observed at 5 and 7%. A very interesting observation from the spectra is that after 7% of  $\text{Tb}^{3+}$  ions, the intensity of the broad band increases further without such increase in the peak at 544 nm, therefore making the spectra complicated. Such a type of complicated spectra had also been reported already by Dai Q and co-workers [3] in  $\text{ZnWO}_4:\text{Eu}^{3+}$  phosphors and they suggested that the origin of the complication is due to the presence of back transfer of energy from  $\text{Eu}^{3+}$  to  $\text{WO}_4^{2-}$ . Therefore it seems that there exists a back transfer of energy from  $\text{Tb}^{3+}$  ions to the host lattice at higher concentrations of  $\text{Tb}^{3+}$  ions. However it is also seen from the figure that the intensity of the broad band increases with the increase of crystallinity. Hence it is suggested that the origin

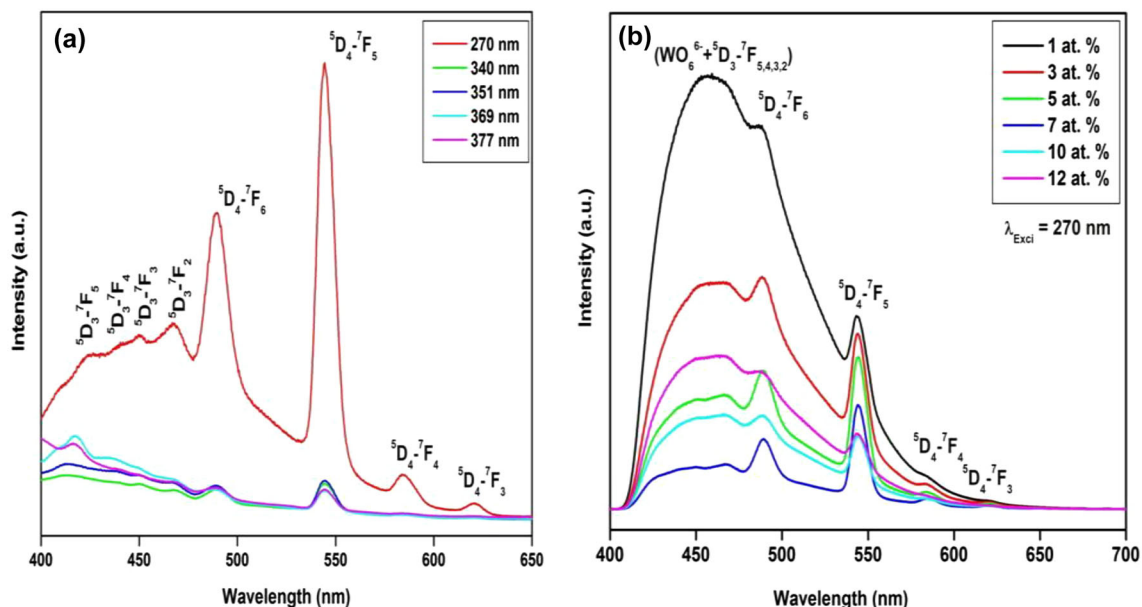


**Figure 5.** (a) Emission spectra of ZnWO<sub>4</sub>:Tb<sup>3+</sup> (7 at%) phosphor at different excitation wavelengths. (b) Emission spectra of ZnWO<sub>4</sub> doped with different concentrations of Tb<sup>3+</sup> ions under excitation at 270 nm.

of this observed complication is due to the combination of the back transfer of energy from Tb<sup>3+</sup> ions to the host lattice and the slight increase in crystallinity. It is revealed from the above results that the concentration of Tb<sup>3+</sup> ions plays an important role in the crystallization and luminescence behaviour of ZnWO<sub>4</sub>:Tb<sup>3+</sup> phosphors.

### 3.5 Lifetime study

The decay curves of all the samples can be well fitted by using the bi-exponential function as:

$$I = I_1 \exp(-t/\tau_1) + I_2 \exp(-t/\tau_2) \tag{1}$$

where  $I_1$  and  $I_2$  are the intensities at two different intervals of times and  $\tau_1$  and  $\tau_2$  are the corresponding decay times. The bi-exponential fitting decay curve of ZnWO<sub>4</sub>:Tb<sup>3+</sup> (7 at%) is shown in figure 6. The bi-exponential decay behaviour of a phosphor is mainly due to three factors such as inhomogeneous distribution of doping ions into the host lattice, transfer of energy from the donor atom and defects present in the host and the presence of impurity [26,34,35]. Then the average lifetime ( $^*\tau$ ) value can be calculated by using the following equation:

$$^*\tau = \frac{I_1 \tau_1^2 + I_2 \tau_2^2}{I_1 \tau_1 + I_2 \tau_2} \tag{2}$$

The average lifetime values calculated by using equation (2) of ZnWO<sub>4</sub>:Tb<sup>3+</sup> for the Tb<sup>3+</sup> concentrations of 1, 3,

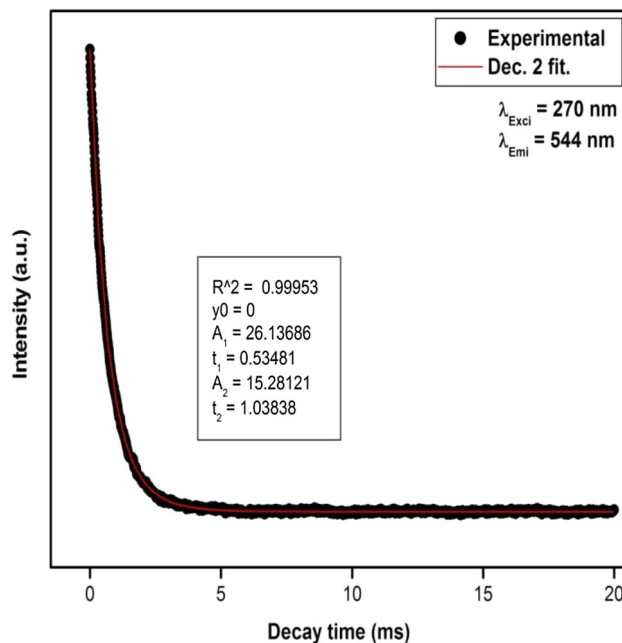


**Figure 6.** Decay curve of ZnWO<sub>4</sub>:Tb<sup>3+</sup> (7 at%) with bi-exponential fitting.

5, 7, 10 and 12% are found to be 1.187, 0.83, 0.814, 0.803, 0.729 and 0.884 ms, respectively, and their goodness of fitting ( $R^2$ ) for the above concentrations is 0.99949, 0.99957, 0.99961, 99953, 99474 and 0.9929, respectively. The above lifetime values of Tb<sup>3+</sup> well agree with those reported by Jinsheng *et al* [34]. The lifetime values are

found to decrease with the increase of the  $Tb^{3+}$  ion concentration, which may be due to the concentration quenching effect.

#### 4. Conclusion

Nanophosphors of  $Tb^{3+}$  ion doped  $ZnWO_4$  have been prepared successfully by the co-precipitation method using ethylene glycol as the reaction medium and the capping agent followed by heat treatment of the precipitates formed at  $500^\circ C$  for 2 h. The TEM image of  $ZnWO_4:Tb^{3+}$  (7%) phosphors showed a spherical shape with a diameter of the crystallites approximately in the range of 8–12 nm. The crystallinity of the samples was found to decrease with the increase of  $Tb^{3+}$  ion concentration due to the deterioration in the crystal lattice. The photoluminescence studies showed a broad band in the blue region due to the charge transfer transition within the  $WO_6^{6-}$  group besides narrow and sharp peaks corresponding to the electronic transition within the 4f energy levels of  $Tb^{3+}$  ions. The concentrations of  $Tb^{3+}$  ions showed a strong influence on the emission behaviour and the high efficient energy transfer from the host lattice to  $Tb^{3+}$  ions was observed at 5 and 7%. The decay time analysis showed bi-exponential fitting and 1% was found to be the maximum average lifetime. From the above results it is believed that these phosphors may have potential applications in lighting and display devices for the production of bluish-green or green colour.

#### Acknowledgements

The authors are very thankful to the sophisticated analytical instrument facility (SAIF), NEHU, Shillong, India, for providing TEM, HRTEM and SAED facilities. The authors are also very thankful to the University science instrumentation center (USIC), University of Delhi, India, for providing FTIR facility.

#### References

- [1] Zhang J, Zhao T, Wang B, Li L, Zou L and Gan S 2015 *J. Phys. Chem. Solids* **79** 14
- [2] Victory D C, Phaomei G, Yaiphaba N and Rajmuhon S N 2014 *J. Alloys Compd.* **583** 259
- [3] Dai Q, Song H, Bai X, Pan G, Lu S, Wang T *et al* 2007 *J. Phys. Chem. C* **111** 7586
- [4] Zhai Y, Wang M, Zhao Q, Yu J and Li X 2016 *J. Lumin.* **172** 161
- [5] Tian Y F, Yu P, Xiao D Q, Liu X, Xie R S, Liu Y *et al* 2010 *Ferroelectrics* **402** 89
- [6] Manh H N, Manh A N and Van M N 2012 *Commun. Phys.* **22** 147
- [7] Dai Q, Song H, Pan G, Bai X, Zhang H, Qin R *et al* 2007 *J. Appl. Phys.* **102** 05431
- [8] Siriwong P, Thongtem T, Phuruangrat A and Thongtem S 2011 *CrystEngComm* **13** 1564
- [9] Cao X, Wu W, Chen N, Peng Y and Liu Y 2009 *Sens. Actuators B: Chem.* **137** 83
- [10] You L, Cao Y, Sun Y F, Sun P, Zhang T, Du Y 2012 *Sens. Actuators B* **161** 799
- [11] Jie L, Jun L and Yongfa Z 2007 *Inorg. Chem.* **46** 8372
- [12] Yua C and Yu J C 2009 *Mater. Sci. Eng. B* **164** 16
- [13] Arin J, Dumrongrojthanath P, Yayapao O, Phuruangrat A, Thongtem S and Thongtem T 2014 *Superlattices Microstruct.* **67** 197
- [14] Rahul K S, Anja-Verena M and Pushpal G 2017 *J. Lumin.* **189** 44
- [15] Pushpal G, Rahul K S, Yogendra N C and Anja-Verena M 2017 *RAC Adv.* **7** 33467
- [16] Gayatri S K and Rajmuhon S N 2013 *J. Lumin.* **139** 98
- [17] Dai Q, Song H, Pan G, Bai X, Zhang H, Qin R *et al* 2008 *J. Lumin.* **128** 1205
- [18] Wang L L, Wang Q L, Xu X Y, Li J Z, Gao L B, Kang W K *et al* 2013 *J. Mater. Chem. C* **1** 8033
- [19] Chen X P, Xiao F, Ye S, Huang X Y, Dong G P and Zhang Q Y 2011 *J. Alloys Compd.* **509** 1355
- [20] Wen F S, Zhao X, Huo H, Chen J S, Shu-Lin E and Zhang J H 2002 *Mater. Lett.* **55** 152
- [21] He H Y 2009 *Phys. Status Solidi B* **246** 177
- [22] Ran W, Wang Q, Zhou Y, Ding S, Shi J and Jeong J H 2015 *Mater. Res. Bull.* **64** 146
- [23] Liao J, Zhou D, Qiu X, Liu S and Wen H R 2013 *Optik* **124** 5057
- [24] Shannon R D 1976 *Acta. Cryst. A* **32** 751
- [25] Huang G and Zhu Y 2007 *Mater. Sci. Eng. B* **239** 201
- [26] Gayatri S K and Rajmuhon S N 2013 *New J. Chem.* **37** 2784
- [27] Bhaskar K G, Sivaiah K and Buddhudu S 2010 *Ceram. Inter.* **36** 199
- [28] Jia G, Huang C, Li L, Wang C, Song X, Song L *et al* 2012 *Opt. Mat.* **35** 285
- [29] Yang J, Quan Z, Kong D, Liu X and Lin J 2007 *Cryst. Growth Des.* **7** 730
- [30] Parchur A K, Prasad A I, Ansari A A, Rai S B and Ningthoujam R S 2012 *Dalton Trans.* **41** 11032
- [31] Kesavulu C R, Silva A C A, Dousti M R, Dantas N O, de Camargo A S S and Catunda T 2015 *J. Lumin.* **165** 77
- [32] Sahu N K, Shanta S N, Ningthoujam R S and Bahadur D 2014 *Photonics* **1** 337
- [33] Wang L, Ma Y, Jiang H, Wang Q, Ren C, Kong X 2014 *J. Mater. Chem. C* **2** 4651
- [34] Jinsheng L, Bao Q, Herui W and Weixiong Y 2009 *Opt. Mat.* **31** 1513
- [35] Stouwdam J W and van Veggel F C J M 2002 *Nano Lett.* **2** 733